Surfactant-Assisted Voltage-Driven Silver Nanoparticle Chain Formation across Microelectrode Gaps in Air

Nidhi Shah and Francis P. Zamborini*

Department of Chemistry, University of Louisville, Louisville, Kentucky 40292, United States

ABSTRACT Here we describe the electrodeposition of Ag in the presence of cetyltrimethylammonium bromide (CTAB) onto 5 μm gap Au interdigitated array (IDA) electrodes that are bare, thiol-functionalized, or thiol-functionalized and seeded with 4 nm diameter Au nanoparticles (NPs). After deposition, applying a voltage between 5 and 10 V in air for 0 to 1000 s resulted in one-dimensional (1D) Ag NP chains spanning across the IDA gap. The Ag NP chains form on IDAs functionalized with thiols and Au NP-seeded at about 5 V and at 10 V for the other nonseeded surfaces. Ag NP chains do not form at all up to 10 V when IDAs are treated with ozone or water soaking to remove possible CTA^+ ions from the surface, when Ag deposition takes place in the absence of CTAB, or when the voltage is applied under dry N_2 (low humidity). Chain formation occurs by Ag moving from the positive to negative electrode. Coating the devices with a negatively charged surfactant, sodium dodecyl sulfate, also results in Ag NP chains by Ag moving from the positive to the negative electrodes, which confirms that the chains form by electrochemical oxidation at the positive electrode and deposition at the negative electrode. The surfactant ions and thin layer of water present in the humid environment facilitate this electrochemical process.

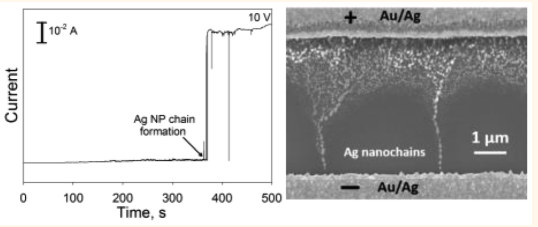

KEYWORDS: silver · nanoparticles · nanochains · one-dimensional · assemblies

Over the past decade, one-dimensional (1D) metal nanoparticle (NP) assemblies have gained widespread attention due to their unique structure, interesting optical and electronic properties, and potential applications.[1−4] These 1D assemblies, also known as nanochains, are of particular interest in plasmonics,[5,6] nanoelectronics,[7] and magnetic devices.[8] They have been utilized in the preparation of solar cells,[9] magnetic memory devices,[10] electronic switches,[11] and sensors.[12,13] Our group is interested in designing simple, low-cost strategies to control the assembly of metallic nanostructures into 1D arrangements and gaining a better fundamental understanding of their electronic and optical properties in order to explore applications in nanoelectronics, sensing, and plasmonics.

There are many methods to synthesize 1D metallic NP assemblies as described in several recent reviews.[1−3,13−17] One of the most common methods is the use of linear templates to direct the 1D assembly. Linear template methods include hard and soft templates. Anodized aluminum oxide (AAO) membranes, polycarbonate membranes, carbon nanotubes (CNTs), amorphous carbon, and zeolite materials are all examples of hard templates, where 1D metal nanochains are formed by filling the pores or cavities of the membrane with metal NPs or by attaching them directly to 1D hard materials so they can align in a 1D fashion. For example, Au NPs have been attached to the walls of CNTs to form 1D nanochains.[18] Sometimes the hard templates are prepared by lithographic methods, such as the etched grooves on the surface of a lithographically micropatterned Si wafer.[19] Soft templates mainly include biological templates and organic polyelectrolytes. DNA has been used most frequently due to its linear structure and ability to attract metal NPs electrostatically.[20−22] Cetyltrimethylammonium bromide (CTAB)-capped Ag NPs were assembled onto a soft DNA template through electrostatic attraction, resulting in 1D Ag NP chains.[23]

Template-free or chemical-based methods involve self-assembly of NPs into 1D nanochains through a variety of interparticle

* Address correspondence to f.zamborini@louisville.edu.

Received for review July 10, 2015 and accepted September 7, 2015.

Published online September 07, 2015
10.1021/acsnano.5b04280

interactions. Multifunctional molecules, such as dithiols, diamines, or polymers, have been used to cross-link metal NPs into 1D assemblies under appropriate conditions. Also, metal NPs can assemble into 1D chains through various intermolecular forces between stabilizers attached to the NPs. Dipole−dipole interactions involving asymmetric charges on individual NPs resulted in 1D assembly following a change in the medium. Linear chains of Au NPs formed when placed in ethanol instead of water, triggered by the different polarity of the medium.[24] Au NPs functionalized with an amphiphilic polymer shell formed 1D chains in solution through van der Waals forces and hydrophobic interactions by adjusting the DMF/H_2O ratio.[25] Hydrogen-bonding interactions[26] and electrostatic interactions have also been used to trigger the formation of Au nanochains.[27,28] The 1D assemblies have been formed by adding a cross-linker, modifying the pH, changing the solvent, or evaporative assembly of NPs from a solution.

Other external forces can be exploited for the preparation of 1D metal NP assemblies, including electric, magnetic, or capillary forces.[14,29] The dipolar attraction caused by a magnetic or electric field is one of the most common and efficient ways to form 1D nanochains. Metal NPs with magnetic properties spontaneously align into 1D chain structures due to the magnetic forces between the particles.[30] 1D assemblies of metal NPs can be achieved by placing the NPs in an alternating current (ac) electric field through polarization of the conductive metal NPs.[31] Capillary forces between NPs can result in 1D assembly during evaporation of solvent.

The surfactant CTAB has been previously used to electrostatically assemble metal NPs into 1D arrays.[32,33] An appropriate concentration of CTAB served as glue that linked neighboring NPs, resulting in short 1D nanochains. Nogami and co-workers[26,34] studied the synthesis of Au and Ag nanochains in this manner and their use in surface-enhanced Raman spectroscopy (SERS). In another study, Sau and Murphy[35] explained that the CTAB molecules come close together by sharing a common layer of counterions or by interdigitation of CTAB tails from neighboring NPs to form 1D assemblies. The assemblies formed spontaneously from a solution of NPs.

Several groups have reported on the use of electric fields to form 1D assemblies across two separated metal electrodes. Dielectrophoresis (DEP)[36−40] involves the generation of an ac electric field between two electrodes in the presence of a solution of the NPs to direct the assembly. The metal NPs become polarized when placed in the electric field. The charge created on the surface of the metal NPs interacts with the nonuniform electric field and produces a dipole, where one end of the dipole experiences a stronger electric field than the other, leading to 1D assembly. Stellacci *et al.*[37] reported the controlled 1D assembly of 20 nm Au NPs with interesting electronic properties into nanogaps using DEP. Chains of various sized Au NPs were assembled between nanoscale and microscale electrodes using an ac electric field in combination with a template that the NPs could be drop-coated into.[36] Metal NPs have also been assembled from a liquid suspension into microwire electrical connections in the form of pearl chains by DEP.[41] DEP offers the opportunity to selectively place metal nanostructures inside electrically defined gaps with good control.

Here we combine the use of CTAB and electric fields to form 1D Ag nanochains between two electrodes. Our group previously used an electrochemical approach to grow 1D Ag NWs across electrode gaps to form electrode/Ag nanowire/molecule/electrode junctions[42] for potential use in electronic-based sensing, molecular electronics, or combined electronic and surface-enhanced Raman spectroscopy measurements.[43,44] In this work we electrochemically deposited Ag onto 5 μm gap Au interdigitated array (IDA) electrodes or a 5 μm gap Au two-electrode device (TED) as in our previous work, but in the presence of CTAB, which led to Ag NPs on the IDA electrodes instead of NWs. Subsequent application of 5−10 V to the IDA in air led to the formation of 1D Ag NP chains connecting the electrode gaps. The mechanism is electrochemical and therefore quite different than previous electrophoretic mechanisms. It is unique in that it occurs in humid air instead of solution and more similar to electrochemically driven Ag filament-based resistive switches,[45−49] with the surfactant acting as electrolyte. The voltage required for Ag nanochain formation is relatively low and depends on the treatment of the electrodes, the electrode gap, and amount of CTAB present during Ag electrodeposition. Here we describe the details of the chain formation and potential applications.

RESULTS AND DISCUSSION

As described in the Method section, Ag was electrodeposited onto bare Au, Au/dithiol, or Au/dithiol/AuNPs in the presence of CTAB at a potential of −0.2 V for 1−2 h as needed on one or both leads of the Au IDA or TED to deposit about 3.0×10^{-5} Coulombs of Ag, based on stripping voltammetry. After electrodeposition, we always measured the current between the two terminals of the Au IDA in room air as a function of voltage from +1 V to −1 V as shown in Figure 1. The current of the Au/dithiol/Au NPs device after Ag electrodeposition is at the 20−30 pA level and almost identical to a Au IDA device without any treatment, revealing that there was no connection made across the gap of the device during Ag deposition. The bare Au and Au/dithiol devices all showed the same behavior.

Figure 2 shows SEM images of a bare Au IDA device before (frames A and C) and a Au/dithiol/Au NPs device after Ag deposition (frames B and D). The SEM images confirm that Ag deposited onto the IDA device and that there was no Ag directly connected across the

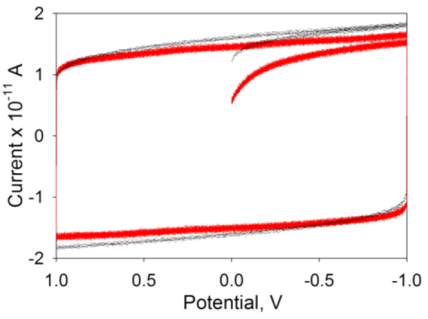

Figure 1. *I*−*V* curve of an untreated bare Au IDA device (gray) and Au/dithiol/Au NPs IDA device after Ag electrodeposition (red). The fact that the current is the same as the bare Au IDA device after Ag electrodeposition shows that the Ag did not make a connection across the 5 μm IDA gap.

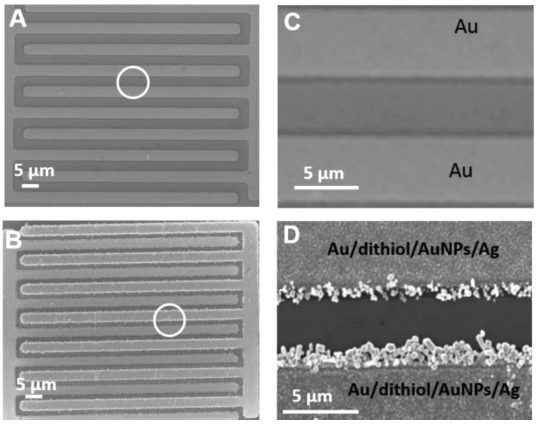

Figure 2. SEM images of (A, C) bare Au IDA device and (B, D) Au/dithiol/Au NPs IDA device after Ag electrodeposition on each side. There is no obvious connection between the two electrodes of the IDA after Ag deposition, which explains the zero current in the *I*−*V* curve of Figure 1. The circled regions in A and B are the regions shown in the magnified images of C and D.

microgaps, explaining the pA level current in the *I*−*V* curve in Figure 1.

Figure 3 shows two-electrode current−time plots at different voltages across the IDA for bare Au (Figure 3A), Au/dithiol (Figure 3B), and Au/dithiol/Au NPs (Figure 3C) IDA devices that had Ag electrodeposited on them in the presence of CTAB. The bare Au and Au/dithiol samples showed a flat 0 current for the first run of 500 s at 5 V. At 10 V, the current increased to the 10^{-3} A level (from pA initially) after 900 s (500 s first run and 400 s second run) and 500−550 s (500 s first run and 50 s second run) for the bare Au and Au/dithiol IDAs, respectively. In contrast, the Au/dithiol/Au NPs IDA sample increased in current to the 10^{-3} A level after about 200 s at 5 V on the first run. The current was spikey initially with drifting in some cases, but eventually stabilized and increased by ~8 orders of magnitude for all samples, but at different voltages and time, depending on the sample treatment.

Figure 4 shows SEM images of the different IDA devices after Ag deposition in the presence of CTAB and application of 5 or 10 V as shown in Figure 3.

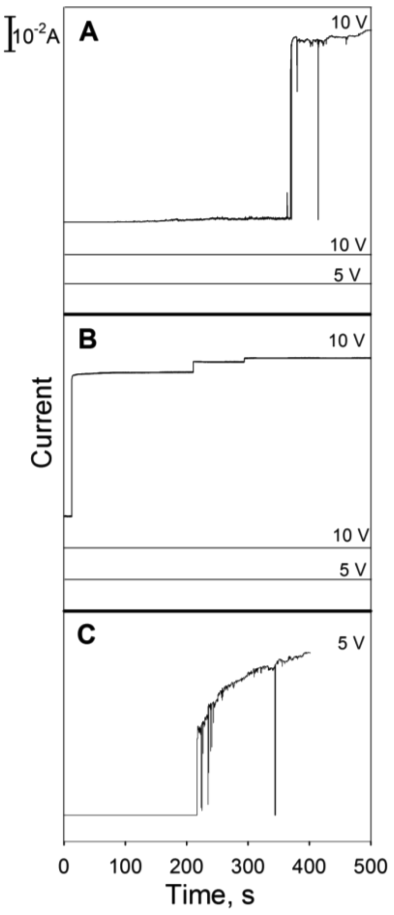

Figure 3. Current−time plots obtained at the indicated voltages on IDA devices with Ag deposited in the presence of CTAB on both sides of (A) bare Au, (B) Au/dithiol, and (C) Au/dithiol/Au NPs devices.

The images also show which electrodes were positive (+) and negative (−) during the applied voltages. From the images, it is clear that the current increased in the Figure 3 *I*−*t* plots due to the formation of Ag NP 1D chains across the 5 μm gap, leading to a conductive pathway for electrons. The chains are wider and some Ag NP material is missing on the (+) electrode, revealing that the formation of the chains occurred by movement of Ag from the (+) electrode toward the (−) electrode. The chains look qualitatively similar other than there is a wider base for the electrodes without the Au NP seeds, although that may not necessarily be reproducible.

We also carried out experiments to deposit Ag on one side of the device to determine if we would still observe Ag NP chain formation. Figure 5 shows current−time plots of devices at 5 and 10 V with Ag deposited in the presence of CTAB on only one side of the Au IDA for bare Au (A), Au/dithiol (B), and Au/dithiol/Au NPs (C) devices, where the side with Ag was the + terminal. There was no current for up to 1000 s at 5 or 10 V for bare Au and Au/dithiol electrodes, while the Au/dithiol/Au NPs device showed several current spikes at 10 V during the 1000 s. The SEM images in

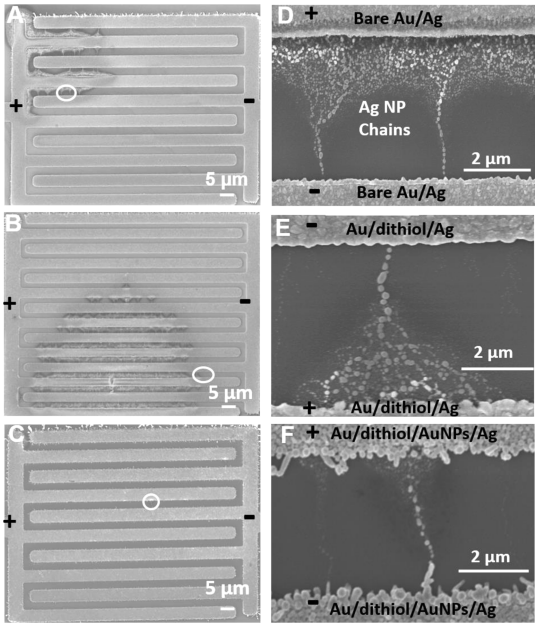

Figure 4. SEM images of various treated IDAs after Ag deposition in the presence of CTAB and application of an applied voltage for various times. (A, D) Bare Au/Ag IDA after applying 5 and 10 V as shown in Figure 3A. (B, E) Au/dithiol/Ag IDA after applying 5 and 10 V as shown in Figure 3B. (C, F) Au/dithiol/Au NPs/Ag IDA after applying 5 V as shown in Figure 3C. Chains of Ag NPs formed across the electrode gap, explaining the large 8−9 order of magnitude increase in current in the *I*−*t* plots in Figure 3. The circled areas are the regions that are expanded in the adjacent SEM images to the right.

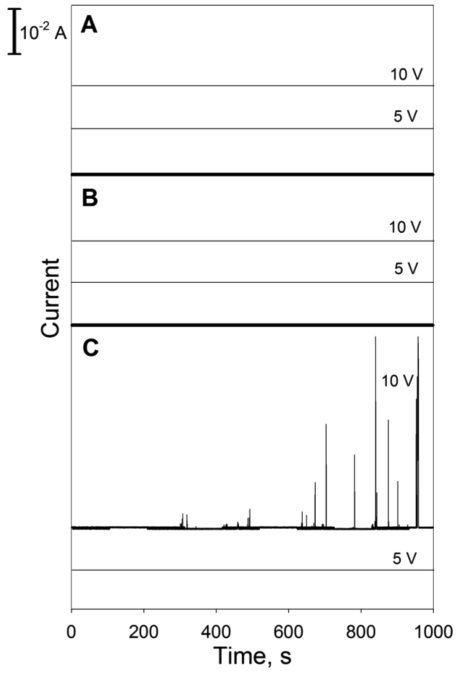

Figure 5. Ag deposition with CTAB on one side of the device. (A) Bare Au/Ag, (B) Au/dithiol/Ag, and (C) Au/dithiol/Au NPs/Ag. The electrode with dithiol, Au seeds, and Ag showed spikes corresponding to Ag NP chain formation after applying 10 V with the Ag side positive.

Figure 6A and B correspond to the device with the current spikes in Figure 5C. These spikes led to the formation of Ag NP chains across the gap similar to that with Ag deposited on both sides. Interestingly, this result shows that when Ag deposition is only on one side of the device, Ag NP chains form at higher voltages compared with Ag deposited on both sides. The higher voltage requirement led to Ag NP chain formation only on the Au/dithiol/Au NPs/Ag (one side) IDA devices. There was no chain formation within 10 V on the bare Au/Ag or Au/dithiol/Ag samples (Ag on one side). Also, a positive voltage had to be applied to the side with Ag to produce chains.

We obtained dark-field microscopy images of Ag NP chain formation across the gap of a two-electrode device on glass with Ag deposited onto Au/dithiol/Au NPs on just one side. The top of Figure 7 shows the current−time plot of the device at 10 V (Ag side positive), and the bottom part shows real-time dark-field microscopy images of the device that corresponds to the current−time plot at different times. This plot showed a very small increase in current around 60 s with no change in the image. A bigger increase in current to about 0.5×10^{-5} to 1.0×10^{-5} A occurred after 95 s that was spikey and a bit unstable. This likely corresponds to the beginning formation of a Ag NP chain across the gap, but the size was too small or not developed enough to observe by optical dark-field microscopy. The Ag NP chain was not observed until about 26 s later at 121 s and was much clearer at 128 s, as shown in Figure 7B. Figure 7A shows the device at 120 s right before the chain became visible. At 128 s the current was still unstable but hovering closer to 2.0×10^{-5} A. About 23 s later a second Ag NP chain was observed faintly but more clearly at 158 s, as shown in Figure 7D (Figure 7C shows the image at 150 s right before the second chain was observed). Overall, these data show that the first chain started forming at 95 s, corresponding to the first step in the current−time plot, but was not visible until 121 s. A current jump occurred as the first Ag NP chain became visible. The current was then spikey and unstable and actually decreased a bit. Another small local current jump occurred as the second chain became visible. The current seemed to increase in interesting step-like jumps that may correspond to the number of chains, but there were also several spikes and unstable current throughout, indicating that the chain formation is a dynamic process. Figure S1 shows more snapshots at times closer to the observation of the two chains, and Figure S2 shows the current−time plot with all of the times marked that correspond to the snapshots. The full video is also included in the Supporting Information. Visualization of each chain occurs over a short time span (~1 s) and clearly occurs by movement of Ag from the positive to the negative electrode, indicated by loss of Ag from the positive side, which is also

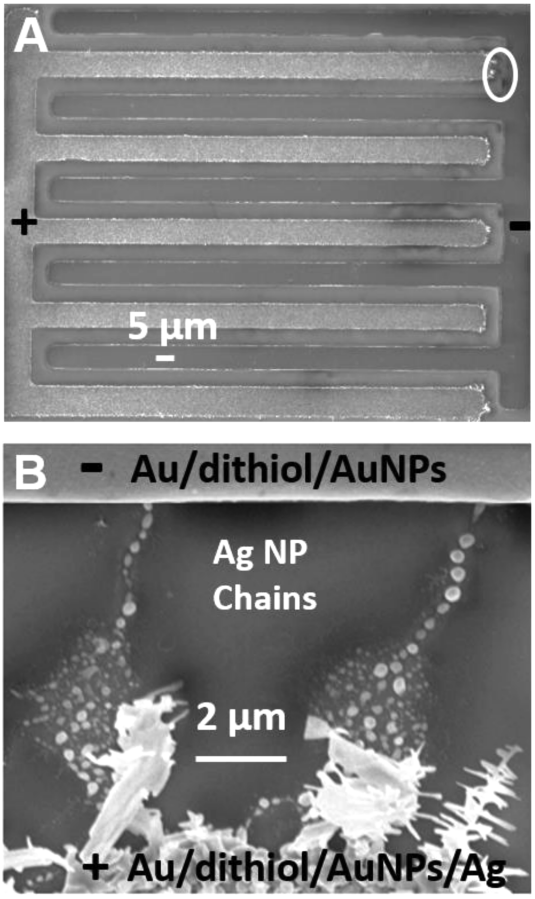

Figure 6. (A) SEM image of an IDA device with Au/dithiol/Au NPs/Ag on one side after application of 10 V (Ag side positive) as shown in Figure 5C. (B) Zoomed-in image of circled part in (A).

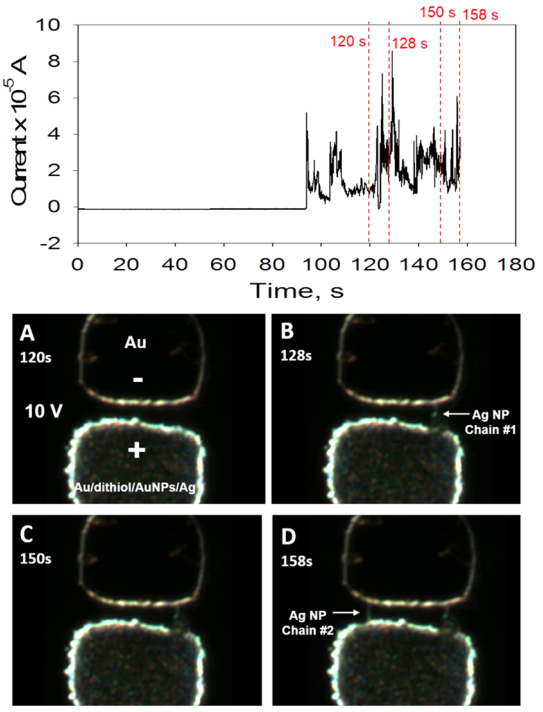

Figure 7. Current–time plot at 10 V (top) and corresponding dark-field microscopy images at (A) 120 s, (B) 128 s, (C) 150 s, and (D) 158 s of a two-electrode device on glass with bare Au on the negative electrode and Au/dithiol/Au NPs/Ag on the positive electrode as indicated in (A). The current increases well before the Ag NP chain can be visualized by dark-field microscopy due to the limited optical resolution. The Ag NP chains start off small and grow with time for 25–30 s until they are visible by dark-field microscopy.

consistent with loss of Ag from the positive electrode observed in SEM images.

Figure 8 shows two Au/dithiol/Au NPs/Ag devices after application of 0.5 V, where one device increased in current to the mA level in about 100 s and another device increased to the mA level in about 450 s. This low voltage was puzzling considering the other devices usually required 5 to 10 V for the current to increase. The SEM images of the device in Figure 8C provided the explanation. The electrodeposition of Ag resulted in Ag dendrites emerging from one of the electrodes in these devices, leading to an effective electrode gap of only about 500 nm. Since the gap was about 10 times smaller in this area, the voltage required to form Ag NP chains was also about 10 times smaller. This shows that the voltage required to form Ag NP chains is proportional to the electrode gap size.

Control experiments conducted with Ag deposited on Au, Au/dithiol, and Au/dithiol/Au NPs (one or two sides) in the absence of CTAB showed no Ag NP chain formation at all up to 10 V for over 1000 s (Figure S3, Supporting Information). This shows that CTAB is critical to Ag NP chain formation, which we believed was due to adsorbed CTAB on the surface. To further support this, we prepared two devices with electrodeposited Ag in the presence of CTAB onto the Au/dithiol/Au NPs IDA (one side only) and then soaked one device in water for 2 h and treated the other device with ozone for 15 min. If the samples contained adsorbed CTAB, which is critical to Ag NP chain formation, then soaking and ozone treatments would likely remove CTAB and we would not observe chain formation in the 0 to 10 V range (Ag side positive). These control experiments did not show any Ag NP chain formation at all up to 10 V for over 1000 s (Figure S4, Supporting Information), further supporting that adsorbed CTAB is important for Ag NP chain formation.

We also studied the role of humidity on Ag NP chain formation. Figure 9 shows the $I-t$ plot of a Au/dithiol/Au NPs device with Ag deposited on it in the presence of CTAB. Application of 10 V (Ag side positive) for over 1000 s under dry N_2 led to background pA level current, indicating no Ag NP chain formation when under dry N_2. Once the same sample was introduced to humid air later, the current increased to the mA level within 150 s at 5 V, consistent with Ag NP chain formation. This shows that both adsorbed CTAB and humidity are required for Ag NP chain formation.

Since Ag NP chain formation required humidity and CTAB and the chains formed by movement of Ag from

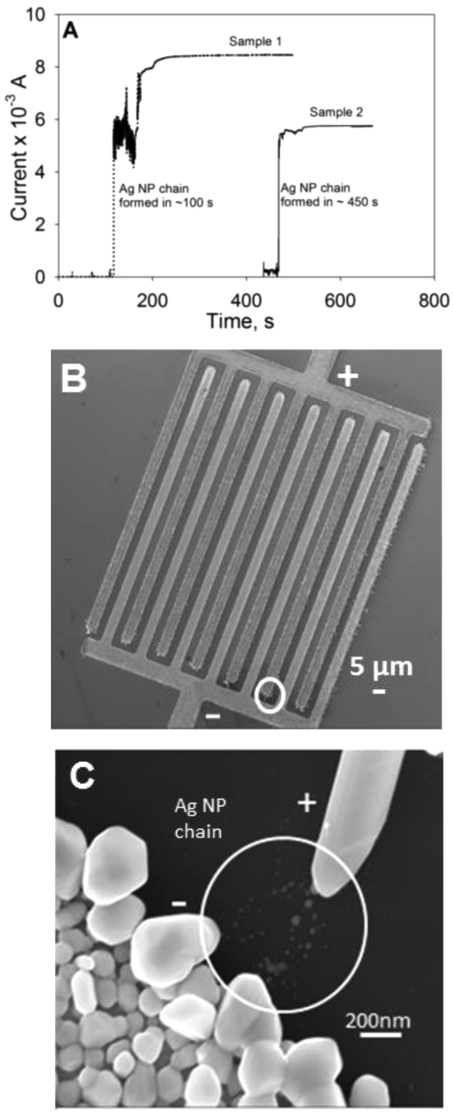

Figure 8. (A) Current−time plot for two Au/dithiol/Au NPs/Ag devices at 0.5 V showing Ag NP chain formation at this low voltage between 100 s and 400 s. (B) SEM image of the device whose current increased after 100 s in (A). (C) Zoomed-in image of the circled part of (B) showing Ag NP chain formation across a much smaller distance, which explains the low voltage required for Ag NP chain formation in this case.

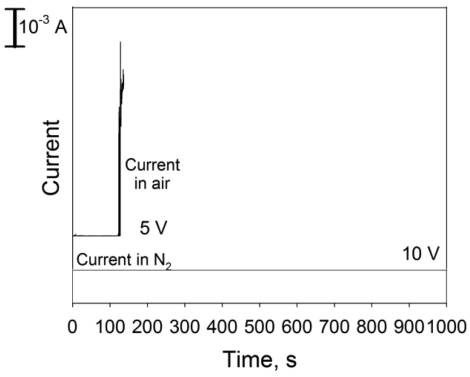

Figure 9. Current−time plots obtained at the indicated voltages on an IDA device with Ag deposited in the presence of CTAB on one side of a Au/dithiol/Au NPs device. The current remained at the instrument background level up to 10 V (Ag side positive) when in the presence of dry N_2. The current increased to the mA level due to Ag NP chain formation once the same device was later introduced to humid air. This shows that humidity is crucial for Ag NP chain formation.

the positive electrode to the negative electrode, we believed that the formation mechanism could be due to either electromigration of positively charged CTA^+-coated Ag NPs from the positive to the negative electrodes or electrochemical oxidation of Ag at the positive electrode and reduction at the negative electrode, where CTAB acts as supporting electrolyte. Both mechanisms could be facilitated by a thin layer of water adsorbed on the device in humid air, depend strongly on adsorbed CTAB, and result in movement of Ag from the positive to negative electrode. The electrochemical mechanism has been described previously in the formation of Ag filaments in resistive switching devices.[45−48,50] To distinguish between these two possibilities, we post-treated Ag-coated Au IDA devices with CTAB, negatively charged surfactant sodium dodecyl sulfate (SDS), and negatively charged citrate ions before applying various voltages in air to determine if Ag NP chain formation would occur in these cases. Soaking a Au/Ag device (Ag on both sides) in 0.1 M CTAB for 1 h, rinsing with water, and drying under nitrogen or soaking in 1.0×10^{-4} M CTAB for 1 h and allowing to air-dry without rinsing resulted in Ag NP chain formation following a 10 and 5 V application, respectively. No Ag NP chains formed with no exposure to CTAB (Figure S5, Supporting Information). As observed when the Ag was deposited in the presence of CTAB, movement of Ag was from the positive to negative electrodes and chain-like structures formed (Figure S6, Supporting Information). Soaking a Au/Ag device in 0.1 M SDS for 1 h, rinsing with water, and drying under nitrogen or soaking in aqueous 1×10^{-4} M SDS for 1 h and allowing it to air-dry without rinsing also resulted in Ag NP chain formation, but following a 4 or 3 V application, respectively (Figure S7, Supporting Information). The movement of Ag was still from the positive to negative electrodes. Soaking a Au/Ag device in 1×10^{-4} M citrate solution for 1 h and allowing it to air-dry without rinsing also resulted in Ag connections across the gap at 3 V (Figure S8, Supporting Information). From SEM images, we found that instead of well-defined Ag NP chains, larger Ag aggregate structures connected the gap, again by movement of Ag from the positive to negative electrode.

For all of the devices soaked or coated with CTAB, SDS, or citrate, we found that the device showed oxidation and reduction peaks when scanning from −1 V to +1 V in air (Figure S9, Supporting Information). The peaks were more prominent for CTAB and SDS. The pair of peaks show clear electrochemical processes occurring on these devices in air. Also, whether the surfactant or ions are positively charged or negatively

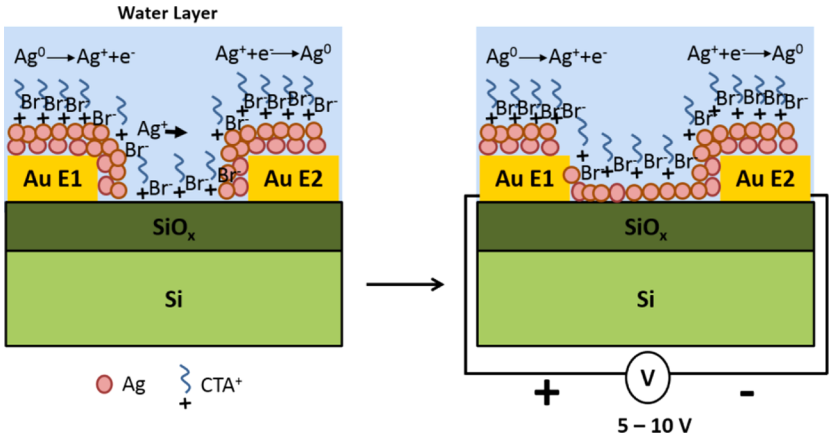

Scheme 1. Illustration of electrochemical Ag NP chain formation mechanism between the two Au electrodes.

charged, the Ag NP chains always formed by movement of Ag from the positive to the negative electrode. We therefore conclude that the Ag NP chain formation is an electrochemical process with the CTAB, SDS, or citrate ions merely acting as supporting electrolyte in a humid environment to facilitate the electrochemical process. This rules out the possibility that CTA^+ ions make the Ag NPs positively charged so that they move by electromigration from the positive to negative electrode. If that was true, then SDS and citrate would make the Ag NPs negatively charged and they would move by electromigration from the negative to the positive electrode, which did not occur. Our data are therefore more consistent with an electrochemical mechanism involving oxidation of Ag to Ag^+ at the positive electrode and redeposition of Ag on the negative electrode by reduction of Ag^+. The voltage required to form the Ag NP chains depends on the electrode gap, but also the amount of surfactant, which explains the variation from 0.5 V for short gaps to 10 V for the larger gaps and the different voltage for one-sided *versus* two-sided devices and different electrode treatment. These all likely lead to different amounts of CTAB on the surface. Increased amount of surfactant and shorter gaps lead to lower resistance to facilitate the electrochemical process.

Scheme 1 illustrates the electrochemical mechanism that we believe leads to Ag NP chain formation. Ag NPs with adsorbed CTAB or other ions are electrochemically oxidized at the positive terminal under the applied potential and then become reduced and redeposit at the negative terminal, eventually connecting the two electrodes in the form of a chain. The growth process of the nanoparticle chains is very similar to the formation of Ag filaments described for resistive switching in other solid electrolyte systems.[11,51−53] Those studies also observed a cylindrical or cone-shaped Ag NP chain feature at the positive electrode and a narrower linear region of the chain at the negative electrode.

CONCLUSIONS

We observed Ag NP chain formation driven by a voltage between electrode gaps separated by as large as a 5 μm distance. We tested bare Au, Au/dithiol, and Au/dithiol/Au NPs (one or two sided) that had $(3.0 \pm 0.3) \times 10^{-5}$ C of Ag electrodeposited on them in the presence of CTAB or that were coated with Ag and untreated or post-treated with CTAB, SDS, or citrate by soaking or drop-coating. After a voltage was applied in humid air, Ag NP chains formed across the microgap due to electrochemical oxidation of Ag to Ag^+ at the positive electrode and redeposition of Ag^+ to Ag at the negative electrode. The surfactant acted as a supporting electrolyte, and the humidity provided a thin water layer on the device to complete the electrochemical cell. No Ag NP chains formed in the absence of these critical components. The voltage required for Ag NP chain formation depended on the amount of surfactant and electrode gap, which varied depending on the electrode treatment method or surfactant treatment method. This work importantly provides a new method for forming Ag NP chains across micrometer-sized electrode gaps in air. Not only can this approach be used to fabricate interesting plasmonic devices, SERS substrates, nanoscale chemiresistors, or resistive switches, it is a useful approach for better understanding the electrochemical formation of metal chain and filament structures in electrochemical systems.

METHODS

Chemicals. Cetyltrimethylammonium bromide (≥97.0%), silver nitrate ($AgNO_3$, ≥99%), trisodium citrate (≥99.0%), and 1,8-octanedithiol (≥97%) were purchased from Sigma-Aldrich. Ethanol (200 proof) was purchased from Decon Laboratories, Inc. Sodium phosphate dibasic (98%) was purchased from EMD Chemicals, and sodium phosphate tribasic (98%) was purchased from Allied Chemicals. NANOpure ultrapure water (resistivity of 18 MΩ-cm) was used for all aqueous solutions. $HAuCl_4 \cdot 3H_2O$ was synthesized from metallic Au.

Electrode Devices. Interdigitated array electrodes with a 5 μm gap or two-electrode devices were used for these studies. These devices were fabricated in a clean room by photolithography on a Si/SiO_x substrate and wired as described previously.[42] The two Au electrodes of the devices were cleaned by rinsing in acetone, ethanol, 2-propanol, and nanopure water and drying under nitrogen. They were used (1) directly after cleaning (termed "bare Au"), (2) after cleaning and placing in a 2 mM ethanolic 1,8-octanedithiol solution for 0.5 h, rinsing with ethanol and water, and drying under N_2 (termed "Au/dithiol"), or (3) after cleaning, functionalizing with 1,8-octanedithiol as already described, and soaking in a solution of 4 nm diameter Au NPs for 20 min, followed by rinsing with water and drying under N_2 (termed "Au/dithiol/Au NPs"). The 4 nm diameter Au NPs were prepared as described by Murphy and co-workers.[54,55]

Electrodeposition. Electrodeposition of Ag was performed on the differently prepared Au IDA electrodes by connecting one side of the IDA device as the working electrode and placing it into a beaker with a solution containing 2.5×10^{-4} M $AgNO_3$ and 0.1 M CTAB in pH 10.6 phosphate buffer with a Ag/AgCl reference electrode and platinum wire counter electrode to complete the three-electrode electrochemical cell. The deposition was performed in cyclic voltammetry mode by scanning the potential from +400 mV to −200 mV and then pausing at −200 mV for 1 h. After 1 h, the deposition was stopped and performed the same way on the other side of the IDA. After, the Au IDA device was removed from solution, rinsed thoroughly with nanopure water, and dried under a gentle flow of nitrogen. We performed stripping voltammetry to measure the charge of Ag on both sides of the IDA to quantify the amount of Ag, which was approximately $(3.0 \pm 0.3) \times 10^{-5}$ C. We maintained a similar amount of charge when performing the deposition on the three differently treated IDAs. Ag deposition on Au/dithiol/Au NPs IDAs took 1 h on each side. It took about 1.5 and 2 h, respectively, for Ag deposition on Au/dithiol and bare Au IDAs to maintain the same amount of Ag. Ag deposition was performed for 1.5 h for Au/dithiol/Au NPs devices deposited on only one side.

Ag was also deposited directly onto each side or one side of an electrode device by chronocoulometry at −0.3 V from a solution of 10 mM $AgNO_3$ in water with no other supporting electrolyte until 6×10^{-5} C of charge passed. This led to a compact film of Ag NPs deposited onto each electrode with no dendrites or nanowires. These devices were used to test the effect of Ag deposition without CTAB and for studies involving post-treatment with CTAB and a negatively charged surfactant, SDS, or trisodium citrate. Post-treatment involved soaking the Ag-coated Au electrodes in an aqueous 0.1 M solution of the surfactant or citrate for 1 h, removing, rinsing thoroughly with water, and drying under N_2. Alternatively, the device was soaked in a 1.0×10^{-4} M solution of the surfactant or citrate for 5−10 min, removed, and allowed to air-dry for a few hours without rinsing with water first. This results in a thin drop-cast film of the surfactant on the Ag-coated IDA or TED devices.

Ag Nanoparticle Chain Formation. After electrodeposition of Ag onto both electrodes, or one electrode of the Au IDA, the current was measured as a function of voltage from −1 V to +1 V across the two electrodes using a two-electrode setup. The current measured was always found to be at the pA level (except when post-treated with a drop-cast film of surfactant or citrate), which confirmed that Ag did not electrodeposit directly across the two Au IDA electrodes and make a connection. The pA current level was the same for the Au IDA electrodes before Ag electrodeposition and similar to the two electrodes not hooked up to anything (the instrument noise). Later, the current was measured as a function of time for voltages up to 10 V to trigger 1D Ag nanochain assembly across the IDA gap.

Characterization. The electrodeposition and electrical characterization were performed using a CH Instruments 660A (Austin, TX, USA) electrochemical workstation. The working, reference, and counter electrode leads were used for the three-electrode electrodeposition experiments in solution, and the reference and counter electrodes were shorted together as one electrode and the working electrode as the second electrode for the two-electrode electrical measurements performed in room air or under N_2. Images of the device were obtained using a Carl Zeiss SMT AG Supra 35 VP field-emission scanning electron microscope (FE-SEM). We used resonant Rayleigh dark-field scattering spectroscopy to obtain dark-field images for IDA electrodes fabricated on glass. Dark-field images and the video were obtained with an inverted Nikon Eclipse Ti microscope with a halogen lamp light source and a dark-field condenser (NA = 0.95−0.80) for sample illumination and a 100× variable-aperture oil immersion objective (NA = 0.5−1.3).

Conflict of Interest: The authors declare no competing financial interest.

Acknowledgment. We gratefully acknowledge the National Science Foundation (CHE-1308763) for full financial support of this research. We would also like to acknowledge Robert Cohn and Tereza Paronyan of the Huson Nanotechnology Core Facility at the University of Louisville for providing access and training on the scanning electron microscope used in these studies.

Supporting Information Available: The Supporting Information is available free of charge on the ACS Publications website at DOI: 10.1021/acsnano.5b04280.

Additional snapshots at various times, control experiments for devices prepared in the absence of CTAB, and the effect of post-treatment of devices with CTAB, SDS, and citrate on the Ag NP chain formation (PDF)
Real-time dark-field microscopy video of Ag NP chain formation (MPG)

REFERENCES AND NOTES

1. Tang, Z.; Kotov, N. A. One-Dimensional Assemblies of Nanoparticles: Preparation, Properties, and Promise. *Adv. Mater.* **2005**, *17*, 951–962.
2. Xia, Y.; Yang, P.; Sun, Y.; Wu, Y.; Mayers, B.; Gates, B.; Yin, Y.; Kim, F.; Yan, H. One-Dimensional Nanostructures: Synthesis, Characterization, and Applications. *Adv. Mater.* **2003**, *15*, 353–389.
3. Kitching, H.; Shiers, M. J.; Kenyon, A. J.; Parkin, I. P. Self-Assembly of Metallic Nanoparticles into One Dimensional Arrays. *J. Mater. Chem. A* **2013**, *1*, 6985–6999.
4. Nie, Z.; Petukhova, A.; Kumacheva, E. Properties and Emerging Applications of Self-Assembled Structures Made from Inorganic Nanoparticles. *Nat. Nanotechnol.* **2010**, *5*, 15–25.
5. Maier, S. A.; Atwater, H. A. Plasmonics: Localization and Guiding of Electromagnetic Energy in Metal/Dielectric Structures. *J. Appl. Phys.* **2005**, *98*, 011101.
6. Ozbay, E. Plasmonics: Merging Photonics and Electronics at Nanoscale Dimensions. *Science* **2006**, *311*, 189–193.
7. Braun, E.; Eichen, Y.; Sivan, U.; Ben-Yoseph, G. DNA-Templated Assembly and Electrode Attachment of a Conducting Silver Wire. *Nature* **1998**, *391*, 775–778.
8. Corr, S. A.; Byrne, S. J.; Tekoriute, R.; Meledandri, C. J.; Brougham, D. F.; Lynch, M.; Kerskens, C.; O'Dwyer, L.; Gun'ko, Y. K. Linear Assemblies of Magnetic Nanoparticles as MRI Contrast Agents. *J. Am. Chem. Soc.* **2008**, *130*, 4214–4215.
9. Gao, H.; Bao, C.; Yu, T.; Yao, Y.; Li, F.; Yuan, Y.; Liu, J.; Zou, Z. One-Dimensional Assembly of TiO_2 Nanoparticles toward Enhancing Light Harvesting and Electron Transport for Application in Dye-Sensitized Solar Cells. *RSC Adv.* **2014**, *4*, 10519–10524.
10. Liang, Y.; Liu, P.; Yang, G. Fabrication of One-Dimensional Chain of Iron-Based Bimetallic Alloying Nanoparticles with Unique Magnetizations. *Cryst. Growth Des.* **2014**, *14*, 5847–5855.
11. Sun, H.; Liu, Q.; Li, C.; Long, S.; Lv, H.; Bi, C.; Huo, Z.; Li, L.; Liu, M. Direct Observation of Conversion between Threshold Switching and Memory Switching Induced by Conductive Filament Morphology. *Adv. Funct. Mater.* **2014**, *24*, 5679–5686.
12. Cui, Y.; Björk, M. T.; Liddle, J. A.; Sönnichsen, C.; Boussert, B.; Alivisatos, A. P. Integration of Colloidal Nanocrystals into

Lithographically Patterned Devices. *Nano Lett.* **2004**, *4*, 1093–1098.
13. Liu, S.; Tang, Z. Nanoparticle Assemblies for Biological and Chemical Sensing. *J. Mater. Chem.* **2010**, *20*, 24–35.
14. Velev, O. D.; Gupta, S. Materials Fabricated by Micro- and Nanoparticle Assembly – the Challenging Path from Science to Engineering. *Adv. Mater.* **2009**, *21*, 1897–1905.
15. Srivastava, S.; Kotov, N. A. Nanoparticle Assembly for 1D and 2D Ordered Structures. *Soft Matter* **2009**, *5*, 1146–1156.
16. Xu, L.; Ma, W.; Wang, L.; Xu, C.; Kuang, H.; Kotov, N. A. Nanoparticle Assemblies: Dimensional Transformation of Nanomaterials and Scalability. *Chem. Soc. Rev.* **2013**, *42*, 3114–3126.
17. Walter, M. V.; Cheval, N.; Liszka, O.; Malkoch, M.; Fahmi, A. Hybrid One-Dimensional Nanostructures: One-Pot Preparation of Nanoparticle Chains *via* Directed Self-Assembly of *in Situ* Synthesized Discrete Au Nanoparticles. *Langmuir* **2012**, *28*, 5947–5955.
18. Ellis, A. V.; Vijayamohanan, K.; Goswami, R.; Chakrapani, N.; Ramanathan, L. S.; Ajayan, P. M.; Ramanath, G. Hydrophobic Anchoring of Monolayer-Protected Gold Nanoclusters to Carbon Nanotubes. *Nano Lett.* **2003**, *3*, 279–282.
19. Yin, D.; Horiuchi, S.; Morita, M.; Takahara, A. Tunable Metallization by Assembly of Metal Nanoparticles in Polymer Thin Films by Photo- or Electron Beam Lithography. *Langmuir* **2005**, *21*, 9352–9358.
20. Alivisatos, A. P.; Johnsson, K. P.; Peng, X.; Wilson, T. E.; Loweth, C. J.; Bruchez, M. P.; Schultz, P. G. Organization of 'Nanocrystal Molecules' Using DNA. *Nature* **1996**, *382*, 609–611.
21. Mirkin, C. A.; Letsinger, R. L.; Mucic, R. C.; Storhoff, J. J. A DNA-Based Method for Rationally Assembling Nanoparticles into Macroscopic Materials. *Nature* **1996**, *382*, 607–609.
22. Keren, K.; Krueger, M.; Gilad, R.; Ben-Yoseph, G.; Sivan, U.; Braun, E. Sequence-Specific Molecular Lithography on Single DNA Molecules. *Science* **2002**, *297*, 72–75.
23. Wei, G.; Wang, L.; Zhou, H.; Liu, Z.; Song, Y.; Li, Z. Electrostatic Assembly of CTAB-Capped Silver Nanoparticles along Predefined λ-DNA Template. *Appl. Surf. Sci.* **2005**, *252*, 1189–1196.
24. Liao, J.; Zhang, Y.; Yu, W.; Xu, L.; Ge, C.; Liu, J.; Gu, N. Linear Aggregation of Gold Nanoparticles in Ethanol. *Colloids Surf., A* **2003**, *223*, 177–183.
25. Wang, H.; Chen, L.; Shen, X.; Zhu, L.; He, J.; Chen, H. Unconventional Chain-Growth Mode in the Assembly of Colloidal Gold Nanoparticles. *Angew. Chem., Int. Ed.* **2012**, *51*, 8021–8025.
26. Shiers, M. J.; Leech, R.; Carmalt, C. J.; Parkin, I. P.; Kenyon, A. J. Self-Assembled Ultra-High Aspect Ratio Silver Nanochains. *Adv. Mater.* **2012**, *24*, 5227–5235.
27. Lin, S.; Li, M.; Dujardin, E.; Girard, C.; Mann, S. One-Dimensional Plasmon Coupling by Facile Self-Assembly of Gold Nanoparticles into Branched Chain Networks. *Adv. Mater.* **2005**, *17*, 2553–2559.
28. Sardar, R.; Shumaker-Parry, J. S. Asymmetrically Functionalized Gold Nanoparticles Organized in One-Dimensional Chains. *Nano Lett.* **2008**, *8*, 731–736.
29. Yin, Y.; Lu, Y.; Gates, B.; Xia, Y. Template-Assisted Self-Assembly: A Practical Route to Complex Aggregates of Monodispersed Colloids with Well-Defined Sizes, Shapes, and Structures. *J. Am. Chem. Soc.* **2001**, *123*, 8718–8729.
30. Grzelczak, M.; Vermant, J.; Furst, E. M.; Liz-Marzán, L. M. Directed Self-Assembly of Nanoparticles. *ACS Nano* **2010**, *4*, 3591–3605.
31. Brown, D. A.; Jong-Hoon, K.; Hyun-Boo, L.; Fotouhi, G.; Kyong-Hoon, L.; Wing Kam, L.; Jae-Hyun, C. Electric Field Guided Assembly of One-Dimensional Nanostructures for High Performance Sensors. *Sensors* **2012**, *12*, 5725–5751.
32. Yang, Y.; Shi, J.; Tanaka, T.; Nogami, M. Self-Assembled Silver Nanochains for Surface-Enhanced Raman Scattering. *Langmuir* **2007**, *23*, 12042–12047.
33. Wang, J.-C.; Neogi, P.; Forciniti, D. On One-Dimensional Self-Assembly of Surfactant-Coated Nanoparticles. *J. Chem. Phys.* **2006**, *125*, 194717.
34. Yang, Y.; Matsubara, S.; Nogami, M.; Shi, J.; Huang, W. One-Dimensional Self-Assembly of Gold Nanoparticles for Tunable Surface Plasmon Resonance Properties. *Nanotechnology* **2006**, *17*, 2821.
35. Sau, T. K.; Murphy, C. J. Self-Assembly Patterns Formed Upon Solvent Evaporation of Aqueous Cetyltrimethylammonium Bromide-Coated Gold Nanoparticles of Various Shapes. *Langmuir* **2005**, *21*, 2923–2929.
36. Leiterer, C.; Berg, S.; Eskelinen, A.-P.; Csaki, A.; Urban, M.; Törmä, P.; Fritzsche, W. Assembling Gold Nanoparticle Chains Using an AC Electrical Field: Electrical Detection of Organic Thiols. *Sens. Actuators, B* **2013**, *176*, 368–373.
37. Barsotti, R. J.; Vahey, M. D.; Wartena, R.; Chiang, Y.-M.; Voldman, J.; Stellacci, F. Assembly of Metal Nanoparticles into Nanogaps. *Small* **2007**, *3*, 488–499.
38. Yilmaz, C.; Cetin, A. E.; Goutzamanidis, G.; Huang, J.; Somu, S.; Altug, H.; Wei, D.; Busnaina, A. Three-Dimensional Crystalline and Homogeneous Metallic Nanostructures Using Directed Assembly of Nanoparticles. *ACS Nano* **2014**, *8*, 4547–4558.
39. Kumar, S.; Yoon, S.-H.; Kim, G.-H. Bridging the Nanogap Electrodes with Gold Nanoparticles Using Dielectrophoresis Technique. *Curr. Appl. Phys.* **2009**, *9*, 101–103.
40. Kuzyk, A. Dielectrophoresis at the Nanoscale. *Electrophoresis* **2011**, *32*, 2307–2313.
41. Hermanson, K. D.; Lumsdon, S. O.; Williams, J. P.; Kaler, E. W.; Velev, O. D. Dielectrophoretic Assembly of Electrically Functional Microwires from Nanoparticle Suspensions. *Science* **2001**, *294*, 1082–1086.
42. Dasari, R.; Ibañez, F. J.; Zamborini, F. P. Electrochemical Fabrication of Metal/Organic/Metal Junctions for Molecular Electronics and Sensing Applications. *Langmuir* **2011**, *27*, 7285–7293.
43. Ward, D. R.; Halas, N. J.; Ciszek, J. W.; Tour, J. M.; Wu, Y.; Nordlander, P.; Natelson, D. Simultaneous Measurements of Electronic Conduction and Raman Response in Molecular Junctions. *Nano Lett.* **2008**, *8*, 919–924.
44. Yoon, H. P.; Maitani, M. M.; Cabarcos, O. M.; Cai, L.; Mayer, T. S.; Allara, D. L. Crossed-Nanowire Molecular Junctions: A New Multispectroscopy Platform for Conduction–Structure Correlations. *Nano Lett.* **2010**, *10*, 2897–2902.
45. Waser, R. Redox-Based Resistive Switching Memories. *J. Nanosci. Nanotechnol.* **2012**, *12*, 7628–7640.
46. Waser, R.; Aono, M. Nanoionics-Based Resistive Switching Memories. *Nat. Mater.* **2007**, *6*, 833–840.
47. Waser, R.; Dittmann, R.; Staikov, G.; Szot, K. Redox-Based Resistive Switching Memories – Nanoionic Mechanisms, Prospects, and Challenges. *Adv. Mater.* **2009**, *21*, 2632–2663.
48. Waser, R.; Valov, I. Electrochemical Reactions in Nanoionics - Towards Future Resistive Switching Memories. *ECS Trans.* **2009**, *25*, 431–437.
49. Rosezin, R.; Meier, M.; Breuer, U.; Kugeler, C.; Waser, R. Electroforming and Resistance Switching Characteristics of Silver-Doped MSQ with Inert Electrodes. *IEEE Trans. Nanotechnol.* **2011**, *10*, 338–343.
50. Jin, Z.; Liu, G.; Wang, J. Nonvolatile Resistive Memory Devices Based on Ag. *J. Mater. Chem. C* **2013**, *1*, 3282–3286.
51. Yang, Y.; Gao, P.; Gaba, S.; Chang, T.; Pan, X.; Lu, W. Observation of Conducting Filament Growth in Nanoscale Resistive Memories. *Nat. Commun.* **2012**, *3*, 732.
52. Gao, S.; Song, C.; Chen, C.; Zeng, F.; Pan, F. Formation Process of Conducting Filament in Planar Organic Resistive Memory. *Appl. Phys. Lett.* **2013**, *102*, 141606.
53. Liu, Q.; Sun, J.; Lv, H.; Long, S.; Yin, K.; Wan, N.; Li, Y.; Sun, L.; Liu, M. Real-Time Observation on Dynamic Growth/Dissolution of Conductive Filaments in Oxide-Electrolyte-Based ReRAM. *Adv. Mater.* **2012**, *24*, 1844–1849.
54. Jana, N. R.; Gearheart, L.; Murphy, C. J. Wet Chemical Synthesis of High Aspect Ratio Cylindrical Gold Nanorods. *J. Phys. Chem. B* **2001**, *105*, 4065–4067.
55. Gole, A.; Murphy, C. J. Seed-Mediated Synthesis of Gold Nanorods: Role of the Size and Nature of the Seed. *Chem. Mater.* **2004**, *16*, 3633–3640.